Pulsatory Patterns in Active Fluids

K. Vijay Kumar,[1,2,3] Justin S. Bois,[4] Frank Jülicher,[1] and Stephan W. Grill[1,2,3]
[1]Max Planck Institute for the Physics of Complex Systems, Nöthnitzerstraße 38, 01187 Dresden, Germany
[2]Max Planck Institute of Molecular Cell Biology and Genetics, Pfotenhauerstraße 108, 01307 Dresden, Germany
[3]BIOTEC, Technische Universität Dresden, Tatzberg 47/49, 01307 Dresden, Germany
[4]California Institute of Technology Division of Biology and Biological Engineering, Pasadena, California 91125, USA
(Received 20 December 2013; published 23 May 2014)

We show that pulsatory patterns arise in thin active films in which two chemical species regulate active stress. The regulating species diffuse within the film and are advected by self-generated flows resulting from active stress gradients. Spontaneous pulsatory patterns emerge when the following conditions are met: (i) the fast-diffusing species up-regulates and the slow-diffusing species down-regulates active stress, or (ii) the active stress up-regulator turns over faster compared to the active stress down-regulator. Our study, motivated by pulsatory patterns in the actomyosin cortex in cells and tissues, provides a simple generic mechanism for oscillatory patterns in active fluids.

DOI: 10.1103/PhysRevLett.112.208101 PACS numbers: 87.16.Uv, 87.10.Ca, 87.16.Ln, 89.75.Kd

Pattern formation is an integral part of the development of living systems. Classically, pattern formation in reaction-diffusion systems [1–3] results from chemical instabilities that arise if Turing criteria are satisfied [4]. For example, the interaction between a slow-diffusing activator and a fast-diffusing inhibitor can lead to time-independent spatially periodic patterns. In addition to stationary patterns, bulk oscillations can be generated through specific chemical reaction networks [5]. With spatial degrees of freedom such systems typically generate complex waves but not spatially periodic structures. Spatially periodic oscillatory patterns can result from the coupling of oscillating chemistry with a Turing system [6].

The establishment of patterns in biology generally involves a tight integration of both chemical signals and mechanical events [7–10]. Mechanical events in cells and tissues are typically generated by the cellular cytoskeleton [11]. An important example is actin networks that are driven out of equilibrium by force generation through myosin motor activity. Such networks represent an active material with unconventional material properties [12–15]. Mechanochemical pattern formation processes can arise from the interplay between chemical signals and the active properties of active materials [8]. Recently a general mechanism for the emergence of stationary patterns in active fluids was introduced [10]. Here patterns arise because active stress gradients drive hydrodynamic flows which advect the stress regulator and counterbalance diffusive fluxes.

In this Letter, we study the emergence of *pulsatory patterns* in a thin active film. Our motivation is the pulsatile dynamics in the actomyosin cytoskeleton seen in many morphogenetic processes [16–24]. We consider a system of two chemical species that actively regulate the hydrodynamic stress in a thin film active fluid. Both species are advected by flows resulting from active stress gradients while also diffusing in the thin film. We seek the generic principles underlying the generation of pulsatory patterns in active fluids. Specifically, we ask if there are criteria governing the emergence of pulsatile patterns in active fluids that are analogous to those pertaining to stationary Turing patterns.

We show that a two-component advection-diffusion system coupled to an active fluid in a thin-film geometry leads to the emergence of oscillatory patterns when the fast-diffusing chemical species up-regulates the active stress and the slow-diffusing species down-regulates the active stress. With the inclusion of a simple turn-over reaction for each of the species, oscillatory patterns can also result when the fast turn-over species up-regulates the active stress and the slow turn-over species down-regulates the active stress. These generic Turing-like criteria for active pulsatory patterns represent our key finding. Notably, this mechanism does not require oscillatory chemical instabilities [6,25,26] nor active nematic descriptions with excitable dynamics [27].

Consider two chemical species confined to move in a thin film of finite size L, with concentration fields $A(\mathbf{x}, t)$ and $I(\mathbf{x}, t)$ at position $\mathbf{x}$ and time t, that evolve according to the following advection-diffusion equations:

$$\partial_t A = -\nabla \cdot (\mathbf{v}A) + D\nabla^2 A, \tag{1}$$

$$\partial_t I = -\nabla \cdot (\mathbf{v}I) + \alpha D\nabla^2 I, \tag{2}$$

where D is the diffusion coefficient of species A, $\alpha > 0$ is the ratio of the diffusion coefficients of species I and A, ∇ is the spatial gradient operator, and ∂_t denotes a partial time derivative. We consider both periodic and no-flux boundary conditions. The force-balance condition in the thin film

active fluid leads to a dynamic equation for the hydrodynamic velocity field $\mathbf{v}$ given by [10,17,28]

$$\nabla \cdot \sigma = \gamma \mathbf{v}, \qquad \sigma = \sigma_p + \zeta \Delta\mu \mathbb{1}. \tag{3}$$

Here γ is the friction coefficient describing drag on the substrate (cytosol/plasma membrane). The stress tensor σ is decomposed in a passive contribution

$$\sigma_p = \eta\left[\nabla\mathbf{v} + (\nabla\mathbf{v})^T - \frac{2}{d}(\nabla\cdot\mathbf{v})\mathbb{1}\right] + \eta_v(\nabla\cdot\mathbf{v})\mathbb{1}, \tag{4}$$

and an isotropic active stress $\zeta\Delta\mu$. The shear and bulk viscosities are denoted by η and η_v, respectively [29], and d is the space dimension. We consider the case where the active stress is regulated by the concentrations $\mathbf{c} = (A, I)$ of both chemical species,

$$\zeta\Delta\mu = (\zeta\Delta\mu)_0 f(\mathbf{c}). \tag{5}$$

Here $(\zeta\Delta\mu)_0$ is the active stress amplitude and f a dimensionless function describing active stress regulation.

In this active stress-advection-diffusion system, species A and I are coupled through the advection term stemming from active hydrodynamic flow. Note that the total amounts of A and I are conserved separately. Thus the average concentrations $A_0 = L^{-d}\int d\mathbf{x} A(\mathbf{x},t)$ and $I_0 = L^{-d}\int d\mathbf{x} I(\mathbf{x},t)$ are constant, where L is the system size.

The homogeneous state with concentrations $\mathbf{c}_0 = (A_0, I_0)$ and vanishing velocity $\mathbf{v} = 0$ is a steady-state solution of this model. We perform a linear stability analysis in response to a perturbation of the form $\delta\mathbf{c} \equiv \mathbf{c} - \mathbf{c}_0 = e^{i\mathbf{k}\cdot\mathbf{x}}$ with wave vector $\mathbf{k}$ [1,2]. The spatial Fourier-amplitude of the hydrodynamic velocity field reads

$$\hat{\mathbf{v}}_\mathbf{k} = \frac{i\mathbf{k}(\zeta\Delta\mu)_0(\hat{A}_\mathbf{k}\partial_A f + \hat{I}_\mathbf{k}\partial_I f)}{\gamma(1+\nu k^2\ell^2)}, \tag{6}$$

where we have used Eqs. (3)–(5). The spatial Fourier amplitudes of the concentration fields are denoted $\hat{A}_\mathbf{k}$ and $\hat{I}_\mathbf{k}$ and $\ell = \sqrt{\eta/\gamma}$ is a characteristic length scale. The dimensionless coefficient ν is $\nu = 1$ for $d = 1$ and $\nu = 1 + \eta_v/\eta$ for $d = 2$. Using Eq. (6) in Eqs. (1) and (2) and keeping only linear terms, we find the linear-stability matrix $\mathbb{L}$ with [10]

$$\tau\mathbb{L} = -k^2\ell^2\begin{pmatrix}1 & 0\\ 0 & \alpha\end{pmatrix} + \frac{Pk^2\ell^2}{1+\nu k^2\ell^2}\begin{pmatrix}A_0 f_A & A_0 f_I\\ I_0 f_A & I_0 f_I\end{pmatrix}, \tag{7}$$

where the Péclet number $P = (\zeta\Delta\mu)_0/\gamma D$ is the ratio of the diffusive time scale $\tau = \ell^2/D$ to an advective time scale $\tau_a = \ell/U$ with $U = (\zeta\Delta\mu)_0/\sqrt{\eta\gamma}$, and $f_A \equiv \partial_A f(\mathbf{c}_0)$, $f_I \equiv \partial_I f(\mathbf{c}_0)$. The instabilities of the homogeneous state are determined by the trace $\mathrm{tr}\,\mathbb{L}$ and the discriminant $\Delta\mathbb{L} = (\mathrm{tr}\mathbb{L})^2 - 4\det\mathbb{L}$, where $\det\mathbb{L}$ is the determinant of $\mathbb{L}$ [2]. We find

$$\mathrm{tr}\,\mathbb{L} = -Dk^2[(1+\alpha) - \Pi(k)(A_0 f_A + I_0 f_I)], \tag{8}$$

$$\Delta\mathbb{L} = D^2k^4[(1-\alpha)^2 + \Pi^2(k)(A_0 f_A + I_0 f_I)^2 - 2\Pi(k)(1-\alpha)(A_0 f_A - I_0 f_I)], \tag{9}$$

with $\Pi(k) = P/(1+\nu k^2\ell^2)$. The homogeneous state $\mathbf{c}_0$ is unstable at a wave number k for which the leading eigenvalue $\lambda_+(k)$ of $\mathbb{L}$ is positive. In a system of size L, the wave numbers are $k_n = \omega n\pi/L$ where $n = 0, \pm1, \pm2, \ldots$, and $\omega = 1$ for no-flux and $\omega = 2$ for periodic boundary conditions. From Eq. (8), we find that the mode k_1 becomes unstable first at a critical Péclet number P_c as the Péclet number is increased. From this analysis we obtain the linear-stability diagram shown in Fig. 1. Note that the dynamics become slow in the limit of large systems.

Instabilities can be either stationary or oscillatory. An oscillatory instability occurs when $\mathrm{tr}\,\mathbb{L}(k_1) > 0$ and $\Delta\mathbb{L}(k_1) < 0$. From Eqs. (8) and (9), it follows that for increasing Péclet number, the homogeneous state undergoes an oscillatory instability at

$$P = P_c = \frac{(1+\alpha)(1+\omega^2\pi^2\ell^2\nu/L^2)}{A_0 f_A + I_0 f_I} \tag{10}$$

if $f_A > 0$ and $f_I < 0$ for $\alpha < 1$, or $f_A < 0$ and $f_I > 0$ for $\alpha > 1$. The condition $f_A > 0$ implies that A is a stress up-regulator, while $f_I < 0$ implies that I is a stress down-regulator. Therefore the homogeneous state can undergo an oscillatory instability if the up-regulator of active stress A diffuses faster than the down-regulator I of active stress ($\alpha < 1$) and vice-versa. This criterion for an oscillatory instability in active fluids is reminiscent of a Turing criterion for stationary instabilities in reaction-diffusion systems [4]. However, this instability is mechanochemical in nature and thus fundamentally different from instabilities in reaction-diffusion systems.

To numerically investigate the spatiotemporal oscillation patterns, we choose the active stress regulation function f of the form

$$f(\mathbf{c}) = f_0 + (1+\beta)\frac{A}{A+A_s} + (1-\beta)\frac{I}{I+I_s}, \tag{11}$$

where $f_0 \geq 0$ is the base level and β is an asymmetry parameter in the regulation of active stress, A_s and I_s are the saturation values of the active stress for A and I, respectively. Equation (11) implies that (i) when $\beta < -1$, A down-regulates the active stress and I up-regulates, (ii) when $-1 \leq \beta \leq 1$, both the species up-regulate the active stress and finally (iii) when $\beta > 1$, A up-regulates and I down-regulates the active stress. We emphasize that our results are more general and do not depend on the particular choice of the function f. The results of the linear-stability analysis

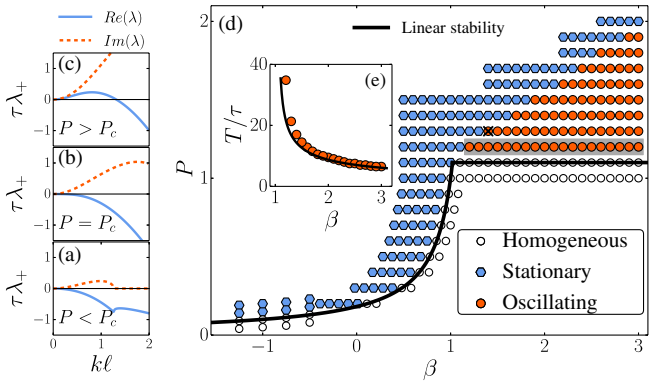

FIG. 1 (Color online) (color online). Dispersion relations and phase diagram for the active stress-advection-diffusion system in $d = 1$ with $\alpha = 0.1$, and using Eq. (11). (a)–(c) Variation of the real and imaginary parts of the leading eigenvalue λ_+ of the linear stability matrix (7) with k for $\beta = 3$, and increasing Péclet numbers P: (a) $P < P_c$, (b) $P = P_c$, and (c) $P > P_c$, where P_c is the critical Péclet number for an oscillatory instability. (d) Phase diagram in the β-P plane. The solid curve is the linear stability boundary for the homogeneous state. The symbols indicate the type of patterns obtained at long times in numerical simulation at different points of the phase diagram (see legend). Temporal snapshots of the dynamics appear in Fig. 2 for the parameter value marked by crossed symbol. Inset (e): Time period of oscillations T determined numerically, for the points enclosed in the gray shaded rectangle in (d), at $P = 1.2$. The solid line is $2\pi/\mathrm{Im}[\lambda_+(k_1)]$.

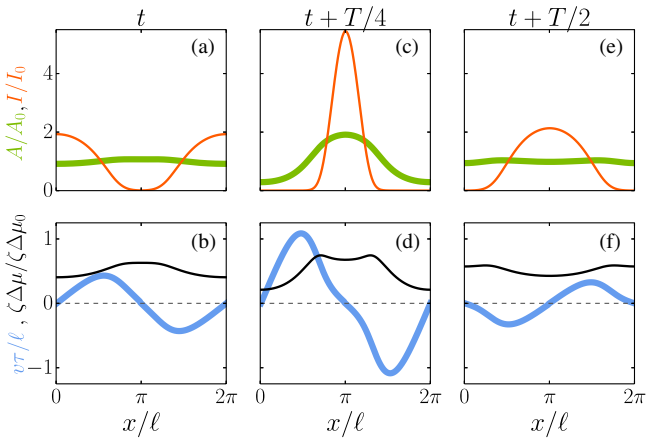

FIG. 2 (Color online) (color online). Temporal evolution of the active stress-advection-diffusion model in $d = 1$ with parameter values corresponding to the point marked with crossed symbol, Fig. 1(d). The top row (a,c,d) shows the evolution of the concentration profiles of A (thick green curve) and I (thin red curve) for half a period. Time points are specified above the plots. The bottom row (b,d,f) shows the corresponding profiles of the hydrodynamic velocity v (thick blue curve) and the active stress $\zeta\Delta\mu$ (thin black curve). The Supplemental Material [30] contains a movie showing the temporal evolution of these profiles.

depend only on the derivatives of f evaluated at the homogeneous fixed point $\mathbf{c}_0$

Figures 1(a)–(c) display the variation of the real and imaginary parts of the leading eigenvalues λ_+ as a function of wave number k for $\beta = 3$. As the Péclet number increases, the system undergoes an oscillatory instability. To investigate the oscillating states, we numerically solved the Eqs. (1)–(5) in a periodic domain of size $L = 2\pi$ in $d = 1, 2$, starting with small random perturbations about the homogeneous state $\mathbf{c}_0$. We also chose $f_0 = 0$, $A_s = \xi A_0$, $I_s = \xi I_0$, with $\xi = 3$ and multiplied the function f by a factor $(1 + \xi)^2/\xi$. The results of the numerical simulations, in $d = 1$ and with $\alpha = 0.1$, are shown in Fig. 1(d). The time period of the oscillation patterns T close to the instability will be inversely proportional to the imaginary part of growth rate $\mathrm{Im}[\lambda_+(k_1)]$. Figure 1(e) compares the time period of the oscillations as determined in numerical simulations with that from the linear stability analysis. It is interesting to note that for large enough P (and $\beta > 1$), the oscillatory patterns are unstable and transition to stationary patterns. Note that when the diffusivities of A and I are the same, or when both A and I up-regulate the active stress, the system exhibits stable steady-state patterns as described in Ref. [10]. We have verified that results of numerical simulations with no-flux boundary conditions also agrees with the linear-stability analysis.

The oscillation mechanism can be understood through simple arguments: a local decrease in I will drive convergent flows towards the depleted region, Figs. 2(a) and 2(b). Flow brings in both A and I, however, I has a lower diffusivity and thus forms a sharper peak, Fig. 2(c). This in turn reduces active stress and the convergent flows, Fig. 2(d). With reduced flow, both peaks in A and I relax by diffusion, however, the I peak remains longer due to the reduced diffusivity of I, Fig. 2(e). This in turn again drives divergent flow away from the remaining peak in I, Fig. 2(f), which serves to accumulate A and I at a different location and repeats the cycle. In summary, the differential regulation of active stress coupled with different diffusive relaxation time-scales lead to pulsatory patterns.

Differential relaxation of the concentration fields can also be achieved by introducing distinct relaxation times for A and I through linear chemical kinetics. We thus write

$$\partial_t A = -\nabla \cdot (\mathbf{v}A) + D\nabla^2 A - \kappa(A - A_0), \qquad (12)$$

$$\partial_t I = -\nabla \cdot (\mathbf{v}I) + D\nabla^2 I - \rho\kappa(I - I_0), \qquad (13)$$

where κ is the turnover rate of A, $\rho > 0$ is the ratio of the turnover rate of I to that of A, and A_0 and I_0 are the steady-state values of A and I, respectively, in the homogeneous state. For simplicity, we have now chosen the diffusivities of A and I to be the same. Equations (12) and (13), together with Eqs. (3)–(5) specify our active stress-advection-reaction-diffusion system. Again, A and I are

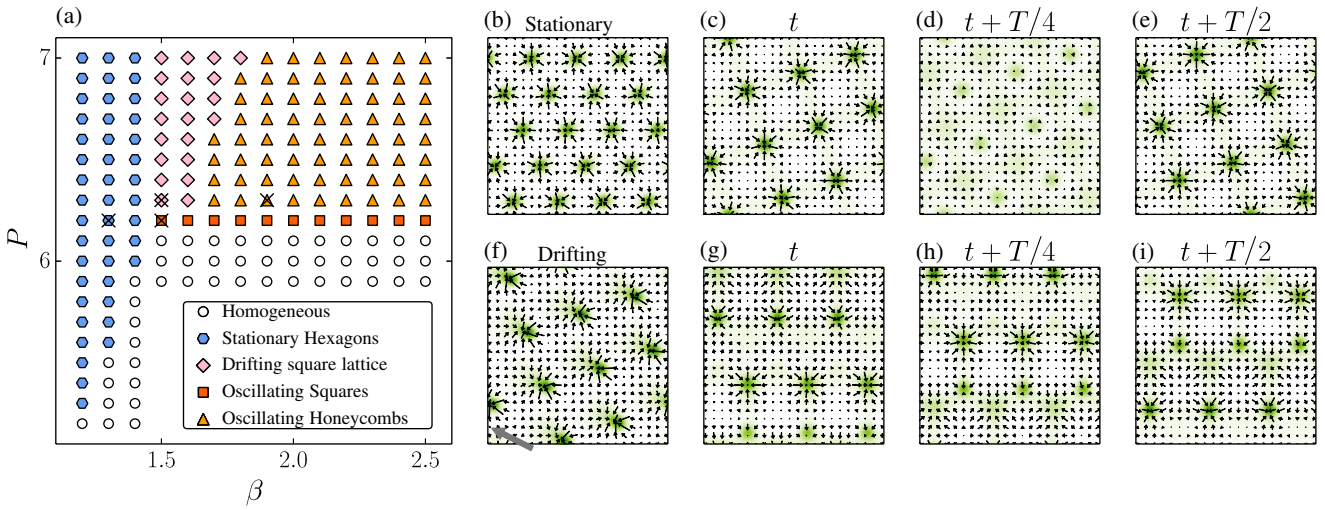

FIG. 3 (Color online) (color online). (a) Phase diagram of the active stress-advection-reaction-diffusion model in $d = 2$ with $\kappa\tau = 1$ and $\rho = 0.1$. (b)–(i) show representative patterns for the points marked with $\times$ in (a). The intensity map represents the concentration field of the species A and the quiver plot represents the hydrodynamic velocity field $\mathbf{v}$. (b) Stationary hexagonal patterns, (c)–(e) temporal evolution of the oscillating square lattice pattern, (f) a drifting square lattice pattern that moves without shape distortion in the direction indicated by the gray arrow, (g)-(i) temporal evolution of the oscillating honeycomb lattice pattern. The Supplemental Material [30] contains movies for the patterns in (b)–(i).

coupled only via advection, and any pattern forming instabilities that may occur are mechanochemical in nature. We analyzed this system in a manner analogous to the previous system, and find that it can exhibit pulsatory patterns when the active stress up-regulator A turns over faster than the active stress down-regulator I, i.e., $\rho < 1$. Figure 3 shows the phase diagram of this system, together with temporal snapshots of the patterns exhibited. The patterns display several maxima arranged in hexagonal patterns for stationary states. In the oscillating phase, we obtain oscillating square lattice patterns or oscillating honeycomb lattice patterns at the points indicated in the phase diagram in Fig. 3. It should be noted that the several maxima that appear in the patterns come about because the ratio of the diffusivity D to the the turnover rate κ sets a length scale, in addition to ℓ.

We have presented a theory for pulsatory patterns in active thin films with two chemical species regulating the active stress. Differential relaxation of the concentrations either via different diffusivities or via different rates of turnover coupled with active stress regulation generically leads to pulsatory patterns. The criteria for oscillatory instabilities are reminiscent of classical Turing criteria for the formation of stationary patterns in reaction-diffusion systems. The mechanism of oscillatory instability involves the chemical regulation of active matter flow and thus is fundamentally different from those observed in chemical systems.

For a system that displays pulsatory patterns, it might be of interest to identify whether pulsation arises due to a purely chemical instability, due to a purely mechanical instability, or due to a combination of mechanics and chemistry. For the first two cases, an analysis of correlations between concentration and flow profiles is adequate to identify them. For example, there are no flows for a purely chemical instability. In an experimental situation, the observed concentration and flow patterns are thus uncorrelated. In the case where neither chemistry nor mechanics alone display pulsatory patterns, they are inseparably coupled to provide the observed dynamic behavior, and must be analyzed as such. In this case, perturbing either chemistry or mechanics will affect the patterns.

Our study was motivated by the pulsatile patterns observed in the actomyosin cytoskeleton. The system with distinct turnover rates is more readily applicable to this case, and the pulsatory patterns that can arise (Fig. 3) share similarities with those observed [16,17,19–21]. Here, myosin motor proteins represent the up-regulating species [17], and it is intriguing to speculate which proteins correspond to the species that down-regulates the active stress. Possibilities are actin itself, or one of the many other proteins that associate with the actomyosin cortex [31]. Although our study was motivated by the pulsatile patterns observed in the actomyosin cytoskeleton, our results are more general and could apply to other systems, for example biological systems at the scale of tissues.

The authors thank A. Saha, G. Salbreux, M. Nishikawa, and S. Naganathan for fruitful discussions. K. V. K. and S. W. G. acknowledge support from the ERC through starting Grant No. 281903. J. S. B. acknowledges the Human Frontier Science Program for funding.

[1] L. Pismen, *Patterns and Interfaces in Dissipative Dynamics* (Springer, Berlin-Heidelberg, 2006).
[2] M. Cross and H. Greenside, *Pattern Formation and Dynamics in Nonequilibrium Systems* (Cambridge University Press, Cambridge, England, 2009).
[3] I. Aranson and L. Kramer, Rev. Mod. Phys. **74**, 99 (2002).
[4] A. M. Turing, Phil. Trans. R. Soc. B **237**, 37 (1952).
[5] I. Prigogine and R. Lefever, J. Chem. Phys. **48**, 1695 (1968).
[6] L. Yang, A. Zhabotinsky, and I. Epstein, Phys. Rev. Lett. **92**, 198303 (2004).
[7] A. Harris, P. Warner, and D. Stopak, Journal of Embryology and Experimental Morphology **80**, 1 (1984).
[8] J. Howard, S. W. Grill, and J. S. Bois, Nat. Rev. Mol. Cell Biol. **12**, 392 (2011).
[9] D. W. Thompson, *On Growth and Form* (Cambridge University Press, Cambridge, England, 1945).
[10] J. S. Bois, F. Jülicher, and S. W. Grill, Phys. Rev. Lett. **106**, 028103 (2011).
[11] J. Howard, *Mechanics of Motor Proteins and the Cytoskeleton* (Sinauer Associates, Sunderland, Massachusetts, USA, 2001).
[12] F. Jülicher, K. Kruse, J. Prost, and J.-F. Joanny, Phys. Rep. **449**, 3 (2007).
[13] J.-F. Joanny and J. Prost, HFSP J. **3**, 94 (2009).
[14] S. Ramaswamy, Annu. Rev. Condens. Matter Phys. **1**, 323 (2010).
[15] M. C. Marchetti, J. F. Joanny, S. Ramaswamy, T. B. Liverpool, J. Prost, M. Rao, and R. A. Simha, Rev. Mod. Phys. **85**, 1143 (2013).
[16] E. M. Munro, J. Nance, and J. R. Priess, Dev. Cell **7**, 413 (2004).
[17] M. Mayer, M. Depken, J. S. Bois, F. Jülicher, and S. W. Grill, Nature (London) **467**, 617 (2010).
[18] S. A. Newman, Mol. Reprod. Dev. **76**, 966 (2009).
[19] A. C. Martin, M. Kaschube, and E. F. Wieschaus, Nature (London) **457**, 495 (2009).
[20] L. He, X. Wang, H. L. Tang, and D. J. Montell, Nat. Cell Biol. **12**, 1133 (2010).
[21] M. Rauzi, P.-F. Lenne, and T. Lecuit, Nature (London) **468**, 1110 (2010).
[22] R. Fernandez-Gonzalez and J. A. Zallen, Phys. Biol. **8**, 045005 (2011).
[23] R. Levayer and T. Lecuit, Dev. Cell **26**, 162 (2013).
[24] C. Westendorf, J. Negrete, A. J. Bae, R. Sandmann, E. Bodenschatz, and C. Beta, Proc. Natl. Acad. Sci. U.S.A. **110**, 3853 (2013).
[25] V. K. Vanag and I. R. Epstein, Phys. Rev. Lett. **92**, 128301 (2004).
[26] V. V. Yashin, O. Kuksenok, P. Dayal, and A. C. Balazs, Rep. Prog. Phys. **75**, 066601 (2012).
[27] L. Giomi, L. Mahadevan, B. Chakraborty, and M. Hagan, Phys. Rev. Lett. **106**, 218101 (2011).
[28] G. Salbreux, J. Prost, and J.-F. Joanny, Phys. Rev. Lett. **103**, 058102 (2009).
[29] In $d = 1$, $\eta = 0$, whereas in $d = 2$ the shear and bulk viscosities for a thin film of an incompressible three-dimensional fluid are related as $\eta_v = 3\eta$. See, for example, A. D. Jenkins and K. B. Dysthe, J. Fluid Mech. **344**, 335 (1997).
[30] See Supplemental Material at http://link.aps.org/supplemental/10.1103/PhysRevLett.112.208101 for movies of the dynamical patterns in Figs. (3b) to Figs. (3i).
[31] T. D. Pollard and J. A. Cooper, Annu. Rev. Biochem. **55**, 987 (1986).